PROGRESSIVE DAMAGE MODEL FOR NON-CRIMP FABRIC COMPOSITE: MODELLING FRAMEWORK AND VERIFICATION

S. A. Rashidi[a,b], H. A. Israr[a]*, S. Othman[b], M. N. Tamin[a]

[a]Faculty of Mechanical Engineering, Universiti Teknologi Malaysia, 81310 UTM Johor Bahru Johor
[b]Aerospace Malaysia Innovation Centre (AMIC)

*Corresponding email: harisahmad@utm.my

Article history
Received
26th May 2025
Revised
15th August 2025
Accepted
2nd September 2025
Published
1st December 2025

ABSTRACT

Non-crimp fabric (NCF) composites have become increasingly used for primary aircraft structures due to its similar mechanical performance as the conventional Carbon Fiber Reinforced Plastic (CFRP) prepreg but comes with a greater manufacturing advantage. Inherent to its manufacturing method such as the Resin Transfer Molding (RTM), the NCF textile comes in dry state and requires stitching to hold the fiber tows in bundle shape for handling purposes. Because of this unique architecture, the damage mechanisms of NCF composites are different compared to unidirectional prepreg, which often comes in tape format. In this study, a progressive damage model operating at mesoscale level is proposed to predict the stiffness and strength of NCF composite laminate. The strength-based model was derived from LaRC05 model with an addition of damage evolution model to account for fracture energy dissipation after damage is initiated. Verification steps were performed using available data on the literature, and comparisons with other damage models such as Hashin model and Tsai-Hill model are conducted to ensure model's conformity and accuracy. The result from the proposed model demonstrates good agreement with experimental data published by other authors with maximum error up to 16%.

Keywords: *Damage Modelling, Non-Crimp Fabric, Finite Element Analysis*

1.0 INTRODUCTION

The carbon fiber Non-Crimp Fabric (NCF) composite is regarded as one of the few alternatives to the conventional Carbon Fiber Reinforced Plastic (CFRP) prepreg for manufacturing aircraft components. Due to its advantages in the manufacturing processes such as easy drapability, shorter curing time, and lower utilities usage, the NCF composites offer a competitive cost solution for complex components such as on the aircraft's primary structures [1], [2].

NCF textile reinforcement typically comes with polyester stitches in both weft and ward directions to maintain unidirectional (UD) alignment of carbon fiber filaments, as shown in Figure 1(a), similar to conventional prepreg UD tape. However, the stitching causes the fibers to bundle into tows, which, when stacked into laminates, can lead to resin pockets and fiber waviness. Several authors have reported the effect of this architecture on the mechanical performance such as stiffness reduction up to 5% and strength reduction up

to 20% [3], [4]. As a result, NCF composites require a distinct approach from conventional UD CFRP prepreg, particularly when it comes to stress and failure analysis.

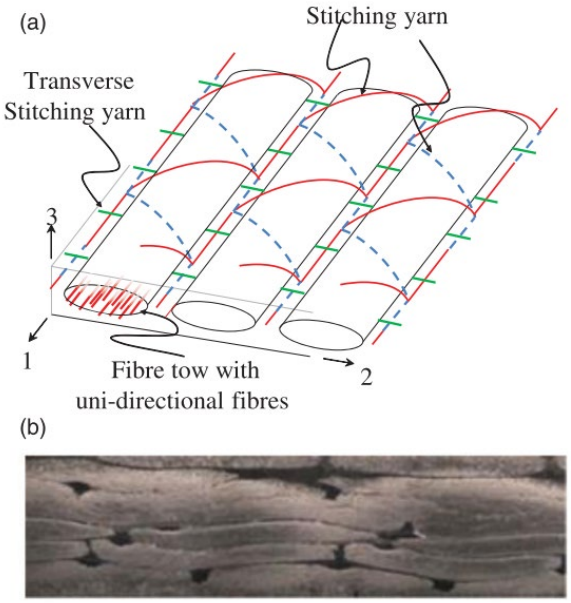

Figure 1: (a) NCF reinforcement textile architecture, (b) cross section of NCF composites [5].

Early investigations [6]–[8] have laid the groundwork for NCF stress and failure analysis by examining the influence of fiber bundle and waviness on mechanical properties. These studies highlighted that the out-of-plane properties to be significantly altered by the textile architecture, with deviation of up to 50% compared to the in-plane properties [9]. This finding indicates that the NCF composites cannot be assumed to be transversely isotropic, thus necessitates full three-dimensional stress consideration. Molker et al. [10] further contributed by proposing a two-mode failure criteria for NCF composite that is capable of distinguishing between in-plane and out-of-plane damage modes. Their model builds upon the LaRC05 failure criteria [11], known for its robustness as demonstrated in Worldwide Failure study [12] and its consideration of in-situ strength effects, which are particularly relevant for NCF composites.

However, most of these works are focused on static loading and assume a total laminate failure once the first-ply failure occurs. In contrast, this paper presents the adaptation of the damage model into a progressive damage framework for NCF composites. This framework incorporates a modified failure criteria and a damage evolution model, capturing both damage initiation and damage evolution via fracture energy dissipation. The models are mainly based on failure criteria developed in [11] and damage evolution model implementation described in [13]. Unlike a study conducted in [14] which employed microscale approach via a Representative Volume Element (RVE) of fiber and matrix to simulate fatigue damage behavior, the progressive fatigue damage in this framework operates at ply level and uses mesoscale lamina properties.

To verify the conformity and accuracy of the framework, a series of verification steps was performed using available data on the literature. The motivation behind the development of the progressive damage model is to enable a more detailed analysis of fracture propagation within the NCF composite laminate through individual element failure. As the damage propagates, we could determine the remaining strength or eventually, the ultimate strength of the laminates.

2.0 MODELLING FRAMEWORK

Describing the progressive damage of Non-Crimp Fabric (NCF) composites necessitates a comprehensive account of different physical phenomena that occur within the plies. This includes the damage initiation phenomenon through a set of failure criteria and the damage progression until complete failure through a damage evolution model.

2.1 Progressive Damage Model of Non-Crimp Fabric (NCF) Composites

In this study, the progressive damage framework for NCF composites utilizes a bilinear damage model to characterize the material's constitutive response, as illustrated in Figure 2. Each unidirectional NCF lamina is considered as homogenous orthotropic layer. The model defines two distinct phases: an initial linear elastic phase followed by a softening phase. In the linear elastic phase leading up to the onset of damage, the material point in governed by the lamina's equivalent elastic properties, as defined by Eq. (1) and (2), where $\Delta = (1 - \mu_{12}\mu_{21} - \mu_{23}\mu_{32} - \mu_{13}\mu_{31} - 2\mu_{21}\mu_{32}\mu_{13})\,/E_{11}E_{22}E_{33}$.

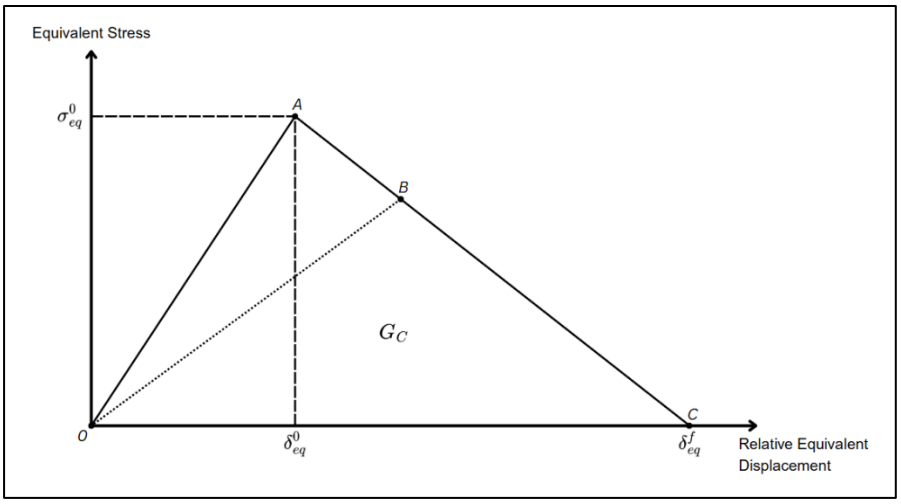

Figure 2: Bi-linear progressive damage model for each failure modes

$$[\sigma] = C.[\varepsilon] \tag{1}$$

$$C = \begin{bmatrix} \frac{1-\mu_{23}\mu_{32}}{E_{22}E_{33}\Delta} & \frac{\mu_{21}+\mu_{23}\mu_{31}}{E_{22}E_{33}\Delta} & \frac{\mu_{31}+\mu_{21}\mu_{32}}{E_{22}E_{33}\Delta} & 0 & 0 & 0 \\ \frac{\mu_{21}+\mu_{23}\mu_{31}}{E_{22}E_{33}\Delta} & \frac{1-\mu_{13}\mu_{31}}{E_{11}E_{33}\Delta} & \frac{\mu_{32}+\mu_{12}\mu_{31}}{E_{11}E_{33}\Delta} & 0 & 0 & 0 \\ \frac{\mu_{31}+\mu_{21}\mu_{32}}{E_{22}E_{33}\Delta} & \frac{\mu_{32}+\mu_{12}\mu_{31}}{E_{11}E_{33}\Delta} & \frac{1-\mu_{12}\mu_{21}}{E_{11}E_{22}\Delta} & 0 & 0 & 0 \\ 0 & 0 & 0 & G_{12} & 0 & 0 \\ 0 & 0 & 0 & 0 & G_{13} & 0 \\ 0 & 0 & 0 & 0 & 0 & G_{23} \end{bmatrix} \tag{2}$$

A set of failure criteria corresponding to each failure mode, as detailed in the following section, is applied as damage initiation criterion (Point *A*). In some analyses, this point is regarded as the catastrophic failure of the composite structure, commonly referred to as first-ply failure. At this stage, the damage state can be physically interpreted as nucleation of voids. Once the damage initiates, the material point transitions into the second state, known as strain softening phase (line *AC*). During this phase, the material point starts to experience a reduction in its stiffness due to micro-voids propagation. With continued loading, these micro-voids evolve into visible cracks, leading to noticeable reduction in the lamina's structural stiffness (Point *B*). Eventually, the cracks propagate further, resulting in a complete material separation (Point *C*).

Much of the work in this phase is rooted in fracture mechanics concept, particularly in describing the softening behavior. A key concept employed is the fracture energy, G_C, a material property that quantifies the amount of energy required to be fully dissipated for a crack to form. This property can be determined either through Eq. (3) or by using a data reduction method, which involves calculating the area under the triangle of a traction-displacement curve where T_0 is the tensile strength and δ_f^I is the displacement at fracture for respective mode *I*.

$$Gc = \frac{1}{2} T_0 \delta_f^I \tag{3}$$

2.2 Failure Criteria of Non-Crimp Fabric (NCF) Composites

Due to its distinctive architecture, the NCF composites are not well-suited to be modelled as transversely isotropic, as properties in the 2-direction differs from those in the 3-direction [9], rendering the plane stress assumption inadequate. To address this limitation, failure criteria capable of evaluating material failure across all three principal laminate directions are required. In this context, Molker et al. [10] proposed a two-mode failure criteria which was based on LaRC05 for NCF composite. This model integrates the original LaRC05 matrix failure criteria with an additional interface damage model. Both components operate in tandem by evaluating stresses acting on the 'potential' fracture plane, rather than the local lamina plane. This approach captures more accurately the contribution of fiber bundle morphology of the NCF laminate, in contrast to conventional prepreg laminates.

2.2.1 Intralaminar failure criteria

The intralaminar failure criteria from LaRC05 were originally developed for the conventional pre-impregnated carbon fiber reinforced plastic (CFRP) composites, for both fiber and matrix damage. One of the key strengths of this model is its flexibility to distinguish different responses in matrix tension and compression (i.e. sand and cast iron). This distinction enables a more accurate representation of matrix behavior under transverse loading conditions. Accordingly, the matrix failure index, denoted as FI_M, is expressed as follows:

$$FI_M = \left(\frac{\tau_{T,M}}{S_T^{is} - \eta_T \sigma_{N,M}}\right)^2 + \left(\frac{\tau_{L,M}}{S_L^{is} - \eta_L \sigma_{N,M}}\right)^2 + \left(\frac{\langle \sigma_{N,M} \rangle_+}{Y_T^{is}}\right)^2 \tag{4}$$

The subscript *M* denotes matrix damage, while the terms τ_T, τ_L, and σ_N correspond to transverse shear stress, longitudinal shear stress and normal stress, respectively, acting on the fracture plane. These stress components are obtained through a stress transformation

procedure outlined in Eq. (5). The third term in Eq. (4) captures the effect of normal stress acting perpendicularly to the (potential) fracture plane which influences the opening or closing of cracks within the matrix. As a result, this failure criterion is applicable for both matrix tensile and compression damage modes.

$$\tau_T = -\frac{\sigma_{22}-\sigma_{33}}{2}\sin(2a) + \tau_{23}\cos(2a)$$

$$\tau_L = \tau_{23}\cos(a) + \tau_{31}\sin(a) \tag{5}$$

$$\sigma_N = \frac{\sigma_{22}+\sigma_{33}}{2} + \frac{\sigma_{22}-\sigma_{33}}{2}\cos(2a) + \tau_{23}\sin(2a)$$

Additionally, the term S_T^{is}, S_L^{is}, and Y_T^{is} represent in-situ transverse shear strength, in-situ longitudinal shear strength and in-situ transverse strength, respectively. These values account for an enhanced shear strength and transverse strength of a ply when it is constrained by surrounding plies with different orientation. In such cases, the stacking sequence plays a critical role in restraining cracks propagation. As a result, these strengths are regarded as structural laminate properties rather than intrinsic lamina properties, as it is influenced by factors such as ply stacking orientation, ply thickness and position within the laminate [15]. For improved accuracy, these in-situ properties can be estimated with linear or nonlinear assumptions, as discussed in [16].

On the other hand, the longitudinal friction coefficient, η_L and transverse friction coefficients, η_T are intrinsic properties of the laminate and need to be determined experimentally. However, in the absence of experimental data, Puck et al. [17] suggest estimating these coefficients using the following relationship:

$$\frac{\eta_L}{S_L} = \frac{\eta_T}{S_T} \tag{6}$$

The values of η_T and transverse shear strength, S_T can also be derived through an expression in function of the fracture plane angle in pure transverse compression, α_0. These relationships are given in Eq. (5) and (6). Additionally, the longitudinal shear strength, S_L can be extracted through an in-plane shear test, such as the ASTM D7078 standard.

$$\tan(2\alpha_0) = -\frac{1}{\eta_T} \tag{7}$$

$$S_T = Y_C\cos(\alpha_0)\left(\sin(\alpha_0) + \frac{\cos(\alpha_0)}{\tan(2\alpha_0)}\right) \tag{8}$$

For fiber damage, FI_F, the failure criteria are based on Hashin criteria [18] and LaRC05 matrix damage model. The subscripts *T* and *C* represent damage in tension and compression, respectively. The fiber failure criteria are given by the following expressions:

$$FI_{FT} = \frac{\langle\sigma_{11}\rangle_+}{X_T} \tag{9}$$

$$FI_{FC} = \left(\frac{\tau_{23}^{m}}{S_T^{is} - \eta_T \sigma_{22}^{m}}\right)^2 + \left(\frac{\tau_{12}^{m}}{S_L^{is} - \eta_L \sigma_{22}^{m}}\right)^2 + \left(\frac{\langle \sigma_{22}^{m} \rangle_+}{Y_T^{is}}\right)^2 \tag{10}$$

2.2.2 Interlaminar failure criteria

Due to the absence of a homogenous, flat interface layer between the NCF plies, as depicted in Figure 1(b), a different approach for interlaminar damage is required, unlike models such as Cohesive Zone Modelling (CZM), which primarily applies to systems with considerably flat interface like in prepreg composite system. The damage model used by [5] is based on the quadratic nominal stress criterion, which is used to assess delamination damage. This is expressed in Eq. (11), with FI_{MI} representing failure index for interface damage.

$$FI_{MI} = \left(\frac{\tau_{T,MI}}{S_{T,MI}}\right)^2 + \left(\frac{\tau_{L,MI}}{S_{L,MI}}\right)^2 + \left(\frac{\sigma_{N,MI}}{Z_T}\right)^2 \tag{11}$$

This failure criterion is applicable only when there is positive normal stress; when $\sigma_{N,MI} \leq 0$, the interface damage, FI_{MI} is set to zero. The presence of positive normal stress is crucial for crack propagation, as it facilitates the creation of two new surfaces between the plies. In contrast, under negative normal stress (compression), the crack will not propagate further, as the stress acts to 'close' the cracks.

2.3 Damage Evolution Model

Once the damage initiation has occurred, the evolution of damage is governed by the damage variables, d_I which describe the dissipation of fracture energy. These variables are calculated using a damage evolution model and are defined by the following expression:

$$d_I = \frac{\delta_{I,eq}^{f}\left(\delta_{I,eq} - \delta_{I,eq}^{0}\right)}{\delta_{I,eq}\left(\delta_{I,eq}^{f} - \delta_{I,eq}^{0}\right)} \tag{12}$$

In this equation, the subscript *I* corresponds to different associated failure modes FT (fiber tension), FC (fiber compression), MT (matrix tension), and MC (matrix compression). The term $\delta_{I,eq}^{f}$ denotes the equivalent displacement at material separation of respective failure mode, and $\delta_{I,eq}^{0}$ is the equivalent displacement at which the damage initiation criterion is satisfied. They can be expressed is Eq. (13) and (14).

$$\delta_{I,eq}^{f} = \frac{2G_I}{\sigma_{I,eq}^{0}} \tag{13}$$

$$\delta_{I,eq}^{0} = \frac{\delta_{I,eq}}{\sqrt{FI_I}} \tag{14}$$

The variable $\sigma_{I,eq}^{0}$ in Eq. (14) corresponds to the stress at damage initiation and G_I is the fracture energy associated with failure modes, *I*. The equivalent displacement, $\delta_{I,eq}$ and equivalent stress, $\sigma_{I,eq}$ are calculated as shown in Table 1, where L_c is the characteristic

length of element that is used to alleviate the strain localization issue due to mesh dependency as described by [19], implemented for 2D elements in [13] and adapted for 3D elements in [20].

Table 1: Equivalent displacement and stress of in-plane failure modes for 3D element

Failure mode, *I*	Equivalent displacement	Equivalent stress
Fiber tensile	$\delta_{FI_{FT},eq} = L_c\sqrt{\langle\varepsilon_{11}\rangle^2 + \alpha{\varepsilon_{12}}^2 + \alpha{\varepsilon_{31}}^2}$	$\sigma_{FI_{FT},eq} = \frac{L_c(\langle\sigma_{11}\rangle\langle\varepsilon_{11}\rangle + \alpha\sigma_{12}\varepsilon_{12} + \alpha\sigma_{31}\varepsilon_{31})}{\delta_{FI_{FT},eq}}$
Fiber compression	$\delta_{FI_{FC},eq} = L_c\langle-\varepsilon_{11}\rangle$	$\sigma_{FI_{FC},eq} = \frac{L_c\langle-\sigma_{11}\rangle\langle-\varepsilon_{11}\rangle}{\delta_{FI_{FC},eq}}$
Matrix tension	$\delta_{FI_{MT},eq} = L_c\sqrt{\langle\varepsilon_{22}\rangle^2 + {\varepsilon_{12}}^2 + {\varepsilon_{23}}^2}$	$\sigma_{FI_{MT},eq} = \frac{L_c(\langle\sigma_{22}\rangle\langle\varepsilon_{22}\rangle + \sigma_{12}\varepsilon_{12} + \sigma_{23}\varepsilon_{23})}{\delta_{FI_{MT},eq}}$
Matrix compression	$\delta_{FI_{MC},eq} = L_c\sqrt{\langle-\varepsilon_{22}\rangle^2 + {\varepsilon_{12}}^2}$	$\sigma_{FI_{MC},eq} = \frac{L_c(\langle-\sigma_{22}\rangle\langle-\varepsilon_{22}\rangle + \sigma_{12}\varepsilon_{12})}{\delta_{FI_{MC},eq}}$
Out-of-plane tensile	$\delta_{FI_{MI},eq} = L_c\sqrt{\langle\varepsilon_{33}\rangle^2 + {\varepsilon_{23}}^2 + {\varepsilon_{31}}^2}$	$\sigma_{FI_{MI},eq} = \frac{L_c(\langle\sigma_{33}\rangle\langle\varepsilon_{33}\rangle + \sigma_{23}\varepsilon_{23} + \sigma_{13}\varepsilon_{13})}{\delta_{FI_{MI},eq}}$

Furthermore, to improve numerical convergence of the simulation and to ensure a gradual and stable degradation of stiffness, a regularized scheme by [21] is adopted. This approach smooths the evolution of damage variables over time and is expressed as:

$$\dot{d}_I^r = \frac{1}{\eta_I}(d_I - d_I^r) \tag{15}$$

Here, $\dot{d}_I^r$ is time-derived regularized damage variable and η_I is viscous coefficient corresponding to the relaxation time for each failure mode. The corresponding viscous coefficient values for each damage mode are tabulated in Table 2. It is important to emphasize that the viscous regularization coefficient, η_I should be kept as small as possible to avoid excessive numerical dampening which may result in artificially delayed damage evolution, thus compromising simulation results. Several studies conducted by various authors [22], [23] suggest a value less than 10^{-3} to avoid altering the physical response of the material.

Table 2: Viscous coefficients used for each damage mode

Coefficient	Damage Modes	Viscous Coefficient Value
η_{FT}	Fiber tensile	0.001
η_{FC}	Fiber compression	0.001
η_{MT}	Fiber tensile	0.0005
η_{MC}	Fiber compression	0.0005

2.4 Material Properties

An experimental study conducted by [24] serves as primary reference in the verification process of the proposed model. The NCF composite laminate used in that study has two configurations as highlighted in Table 3. Although the specific lamina material properties were not explicitly detailed in the study, they were estimated using Composite Laminate Theory (CLT) in combination with Tsai-Hill failure criteria to back-calculate the ultimate laminate strengths. Table 4 below shows the static properties extracted from the manuscript.

Due to the limited information available on the lamina properties, several other relevant information (underlined in the table) is gathered from different studies to complement the required input for the model, especially on the fracture energies.

Table 3: NCF laminate configuration

Specimen	Configuration	Dimensions (mm)			Loading rate
		Width	Length	Thickness	(mm/s)
Cross-Ply (CP)	$[0/90/0/90]_s$	25	125	2.1	1
Angle-Ply (AP)	$[-45/45/-45/45]_s$	25	125	2.1	1

Table 4: Mechanical properties of NCF composite extracted from [9], [24]–[26]

Elastic Properties	Value (GPa)	Strength Properties	Value (MPa)
E_{11}	130	Fiber Ten. Strength, X_T	3500
E_{22}	8.5	Fiber Comp. Strength, X_C	900
E_{33}	8.5	Matrix Ten. Strength, Y_T	80
G_{12}	4.98	Matrix Comp. Strength, Y_C	160
G_{13}	4.98	Out-of-Plane Ten. Strength, Z_T	80
G_{23}	4.7	Out-of-Plane Comp. Strength, Z_C	160
υ_{12}	0.25	In-Plane Shear Strength, S_{12}	65
υ_{13}	0.25	In-Plane Shear Strength, S_{13}	65
υ_{23}	0.45	Out-of-Plane Shear Strength, S_{23}	35
		Fiber Ten. Frac. Energy, Gxt	48
		Fiber Comp. Frac. Energy, Gxc	60
		Matrix Ten. Frac. Energy, Gyt	4.5
		Matrix Comp. Frac. Energy, Gyc	4.5

3.0 MODEL IMPLEMENTATION AND VERIFICATION

The failure criteria and damage evolution model presented in previous sections are adapted and integrated in this study to develop the Progressive Damage Model for Non-Crimp Fabric composites (PDM-NCF). The model is implemented within a Finite Element Analysis (FEA) framework through a user-defined material subroutine. In this section, the finite element implementation is verified against experimental data available in the literature, ensuring its robustness in capturing the damage behavior of NCF composites.

3.1 Implementation of Static NCF Failure Criteria

In this section, the adaptation and integration of failure criteria described in Section 2.2 into the Progressive Damage Model for Non-Crimp Fabric composites (PDM-NCF) is presented. Matrix damage is addressed first, where the failure criteria are expressed as function of the fracture plane angle, α, resulting in distinct expressions for tensile and compression loading conditions. Under transverse tensile loading, the fracture plane angle is assumed to be perpendicular to the load direction, corresponding to a fracture angle $\alpha = 0^{\circ}$. Consequently, Eq. (4) is reformulated for NCF composites matrix tension failure, FI_{MT} as:

$$FI_{MT} = \left(\frac{\tau_{23}}{S_T^{is}}\right)^2 + \left(\frac{\tau_{12}}{S_L^{is}}\right)^2 + \left(\frac{\sigma_{22}}{Y_T^{is}}\right)^2 \tag{14}$$

For matrix compression failure, the failure index FI_{MC} as expressed in Eq. (15) is evaluated through a range of potential fracture plane angles, $\alpha \in [0^{\circ}, 180^{\circ}[$ such that a maximum value is achieved for a given stress state. The $\langle\cdot\rangle_+$ denotes Macaulay bracket, capturing only positive (tensile) part of the stress.

$$FI_{MC} = \left(\frac{\tau_{T,M}}{S_T^{is} - \eta_T \sigma_{N,M}}\right)^2 + \left(\frac{\tau_{L,M}}{S_L^{is} - \eta_L \sigma_{N,M}}\right)^2 + \left(\frac{\langle\sigma_{N,M}\rangle_+}{Y_T^{is}}\right)^2 \tag{15}$$

For fiber damage, simplified criteria based on the Hashin failure model are employed, with the intention of using these in future iteration of the study. The current formulation distinguishes between fiber tension and compression modes, expressed as:

$$FI_{FT} = \frac{\langle\sigma_{11}\rangle_+}{X_T} \tag{16}$$

$$FI_{FC} = \frac{\langle\sigma_{11}\rangle_-}{X_C} \tag{17}$$

The expressions allow for flexible implementation in the scope of the study while maintaining alignment with widely adopted failure theories.

3.2 Model Subroutine Development

The PDM-NCF model is implemented using a user-defined subroutine in a Finite Element Analysis (FEA) software, using the Fortran 90 programming language. The overall process flow for model is shown in Figure 3.

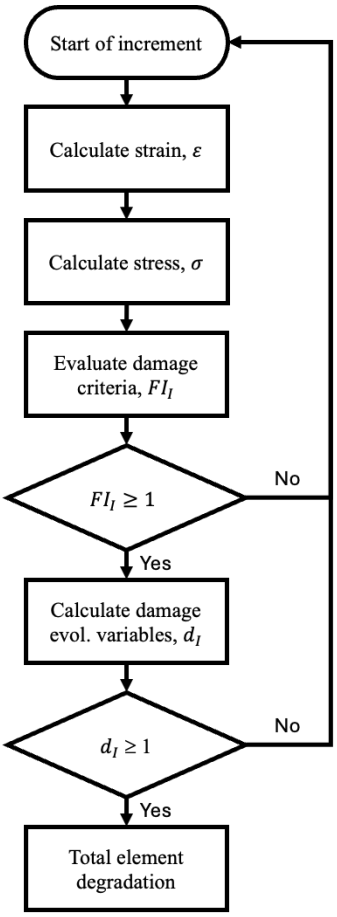

Figure 3: Process flow chart for progressive damage modelling of NCF composites

The user-defined subroutine is developed to leverage the capabilities of the FEA software, which provides essential information such as the current strain increment and time increment. These two variables serve as the primary input to the subroutine. At the start of each increment, the subroutine calls the updated strain values, which are then used to calculate stress components via a 3D constitutive model. The calculated stress components are subsequently used to evaluate Failure Indices (FIs) for the respective failure modes as defined in Eq. (14) to (17).

Once any FI reaches or exceeds a value of unity, the damage evolution is initiated. The associated variable evolves progressively until it reaches a preset threshold value, indicating full dissipation of fracture energy. At this point, the stiffness of affected element is reduced to zero, rendering it inactive. The applied load is then redistributed to the neighboring undamaged elements, allowing the simulation to capture progressive failure behavior.

3.3 Finite Element Model Configuration

Two finite element models are developed to represent the two layup configurations, angle-ply (AP) and cross-ply (CP). Each model is subjected to displacement-controlled tensile loading as shown in Figure 4. The bottom tabbing area is fully constrained (encastre boundary condition) to represent the fixed clamping grip, while top tabbing area is used to apply the tensile load. To ensure unidirectional displacement, a linear-guide boundary

condition is imposed on the side of top tabbing area, restricting lateral movement and allowing only vertical translation.

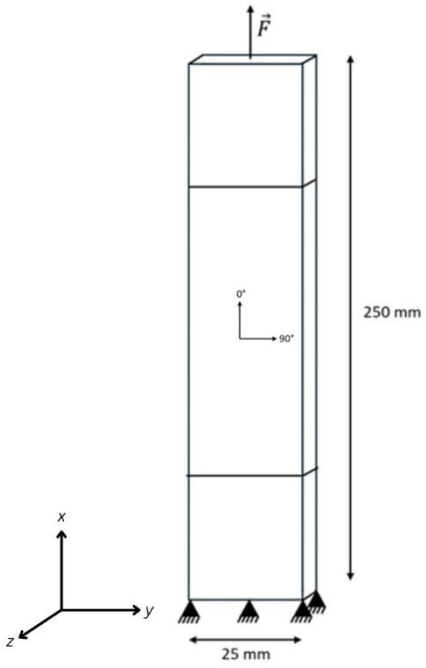

Figure 4: Loading direction, ply orientation and boundary conditions for the NCF laminates

The model utilized 3D elements with three integration points through the thickness, which is necessary due to relatively low ply thickness (0.26 mm) compared to the overall laminate dimensions (height and width). The total laminate thickness is 2.1 mm.

In addition to the user-defined material subroutine, two other damage models are implemented within the numerical study to serve as performance benchmark. These include the FEA software's built-in Hashin damage model and a user-coded Tsai-Hill model. The built-in Hashin damage model supports only continuum shell elements, which limits its application to plane-stress conditions due to the element's intrinsic constitutive behavior. The rest of the damage models utilize full solid elements (C3D8) to fully capture the complete strain and stress tensors in the analysis.

At the current stage of model verification, the interlaminar damage model is not included within the subroutine. This exclusion allows for focused investigation of intralaminar damage analysis which is aligned to the current scope of this research.

3.4 Mesh Convergence Analysis

A mesh convergence analysis is also conducted to ensure that the element size used in the finite element model does not significantly influence the computed variables. The analysis uses tensile strength for the cross-ply laminate and in-plane shear strength for angle-ply laminate as key response variables for the sensitivity analysis. Based on the result of this analysis, an element size of 2 mm is selected for both layup configurations, ensuring the balance between computational efficiency and accuracy.

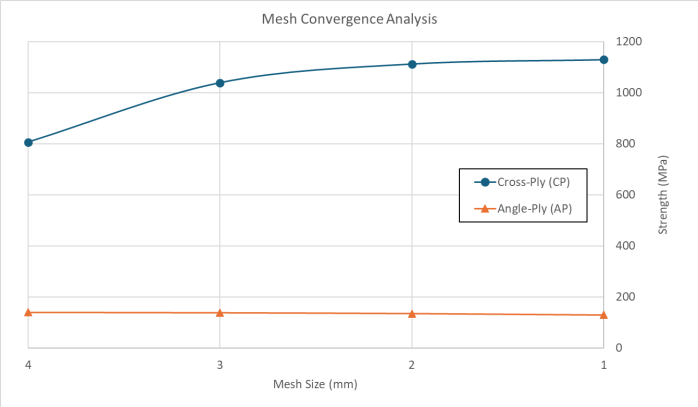

Figure 5: Mesh convergence analysis for both cross-ply (CP) and angle-ply (AP) laminates.

3.5 Model Calibration with Experimental Data

3.5.1 Fracture plane angle under pure transverse compression

The fracture plane angle under pure transverse compression loading, α_0 used in Eq. (5) and (6), depends on the type of composite system that is being used. In this study, unidirectional HTS40 12K NCF fiber from Saertex and RTM6 epoxy resin from Hexcel are used. To accurately represent the transverse friction coefficient, η_T and transverse shear strength, S_T in the FEA model, values extracted from experimental data must be applied. A separate experimental campaign was conducted to obtain this parameter, involving transverse compression testing in accordance with ASTM D3410. The damage morphology from the test is shown in Figure 6. The observed fracture plane exhibits an average angle of 64°, which is adopted in the numerical model.

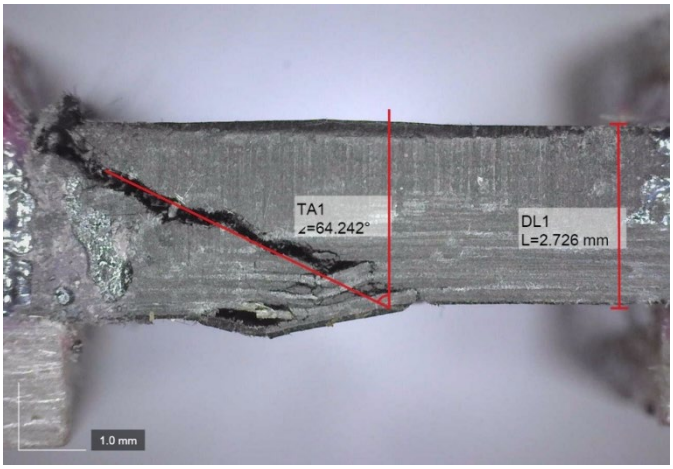

Figure 6: Fracture plane of unidirectional NCF laminate under pure transverse compression loading.

3.5.2 Threshold value of damage evolution variable

Since the experimental fracture energy values presented in Table 4 do not directly represent the composite system employed in this study, the damage evolution model requires proper calibration, particularly regarding its threshold value, which typically corresponds to unity

when full energy dissipation is achieved. A series of numerical experiments are conducted with different threshold values for each failure modes to determine the most suitable threshold limit to be implemented within the progressive damage model.

To calibrate the matrix-driven damage evolution threshold, the experimental results of the angle-ply (AP) specimen were used as benchmark. This choice is justified by the fact that angle-ply laminates are primarily governed by matrix-dominated shear damage when subjected to tensile loading. Figure 7 presents the load-displacement responses comparing different numerical predictions using various matrix damage evolution threshold values. A threshold value of $d_M^r = 0.175$ was found to best replicate complete energy dissipation of matrix-driven damage, achieving the experimental tensile strength of 7.12 kN and effectively initiating stiffness degradation or element deactivation.

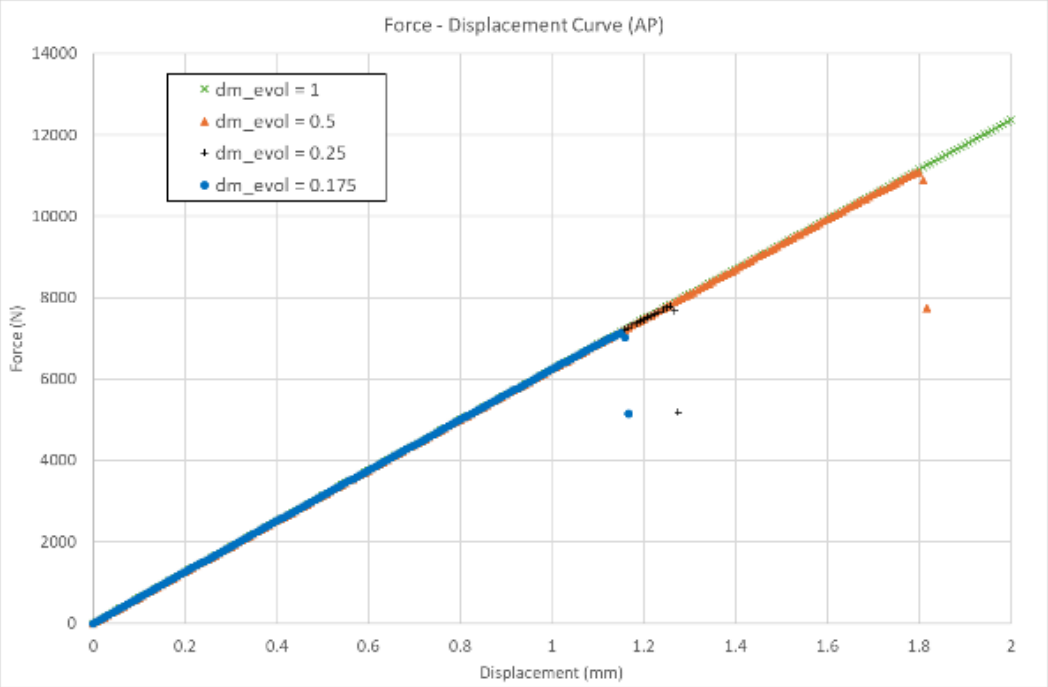

Figure 7: Load-displacement graph of angle-ply (AP) laminate with different matrix damage evolution threshold values.

Meanwhile, a threshold value of $d_F^r = 1$ provided an adequate match for cross-ply (CP) specimens which are predominantly fiber-driven damage and achieve the experimental tensile strength of 58.4 kN. This value works well with the previously selected matrix damage evolution threshold value, ensuring proper damage interaction between different damage modes.

3.5.3 Built-in element deletion feature.

Once the fracture energy within an element is fully dissipated, the element's stiffness should be reduced to zero. At this stage, the element can no longer carry any load, and the applied load is redistributed to neighboring elements. For this load transfer to occur smoothly in the simulation, all integration points within the element must reach their respective damage evolution threshold values. However, when using user-defined element degradation criteria, a challenge arises: as soon as a single (or multiple) integration point reaches the threshold value (i.e. Point 2 and 7) as shown in Figure 8, the solver

automatically reduces the time increment size, towards a level where it becomes unnecessarily small. The step size reduction continues progressively as the solver attempts to resolve the internal stress redistribution across remaining integration points until they achieve complete energy dissipation. This operation becomes computationally expensive, rendering the simulation highly inefficient. An averaging technique could have been implemented; however, the FEA software does not allow user-access for such operation with the integration points.

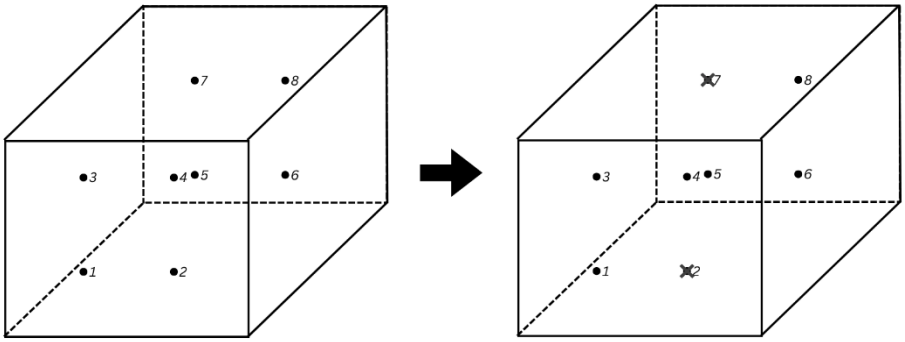

Figure 8: Illustration of some integration points deactivation within a solid 8-node element.

Therefore, to address this limitation, an alternative approach is employed to ensure proper load redistribution among the neighboring elements. The built-in element deletion feature provided within the software is utilized to deactivate fully failed elements. This feature performs averaging technique over all integration points within an element to compute a representative 'centroid' value, which is then used to determine whether the element meets the damage evolution threshold value. The implementation of this feature renders the element not only inactive but also removes it visually from the mesh. Figure 9 illustrates this feature in greater detail.

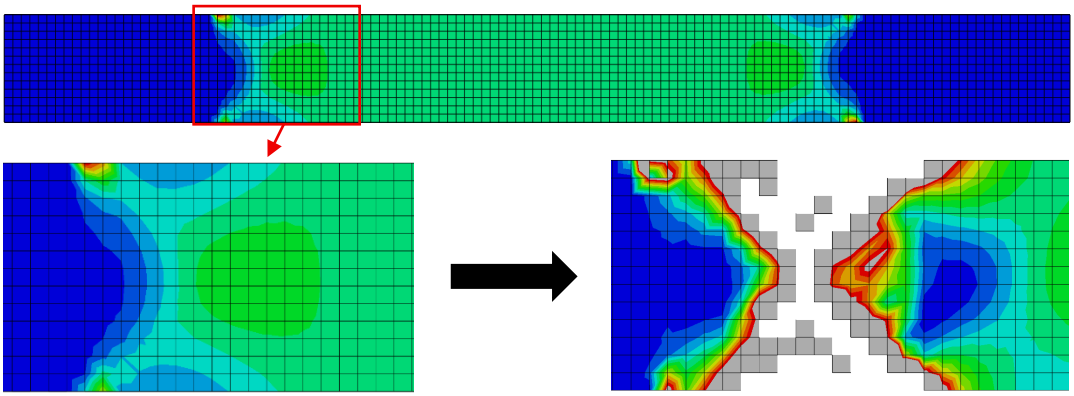

Figure 9: Demonstration of the element deletion feature in the FEA software, element condition when damage initiated (left) and complete failure (right).

4.0 RESULTS AND DISCUSSION

4.1 Stress-Strain Response of the Laminates

For CP laminates, the ultimate failure is mainly driven by fiber damage that is aligned with the loading direction. This damage mode is typically characterized by an abrupt

disintegration of plies into strands of bundled fibers. The overall behavior can be described as elastic-brittle, with a sudden drop in the stress-strain response, as shown in Figure 10.

The experimental stiffness and strength values for CP laminates, as reported by the original author, are 68 ± 3 GPa and 992 ± 25 MPa, respectively. The simulated stiffness value across different models demonstrates good agreement with the experimental result. However, the strength prediction varies depending on the models. The Hashin model has effectively captured the strength drop around 1000 MPa while the PDM-NCF at around 1112 MPa. Notably, the PDM-NCF model requires approximately 13% more strain than Hashin model to reach complete failure. This extended strength and failure strain are attributed to the element's constitutive behavior and the interaction between the damage initiation criteria and damage evolution model which effectively captured a sustained load distribution process before total disintegration.

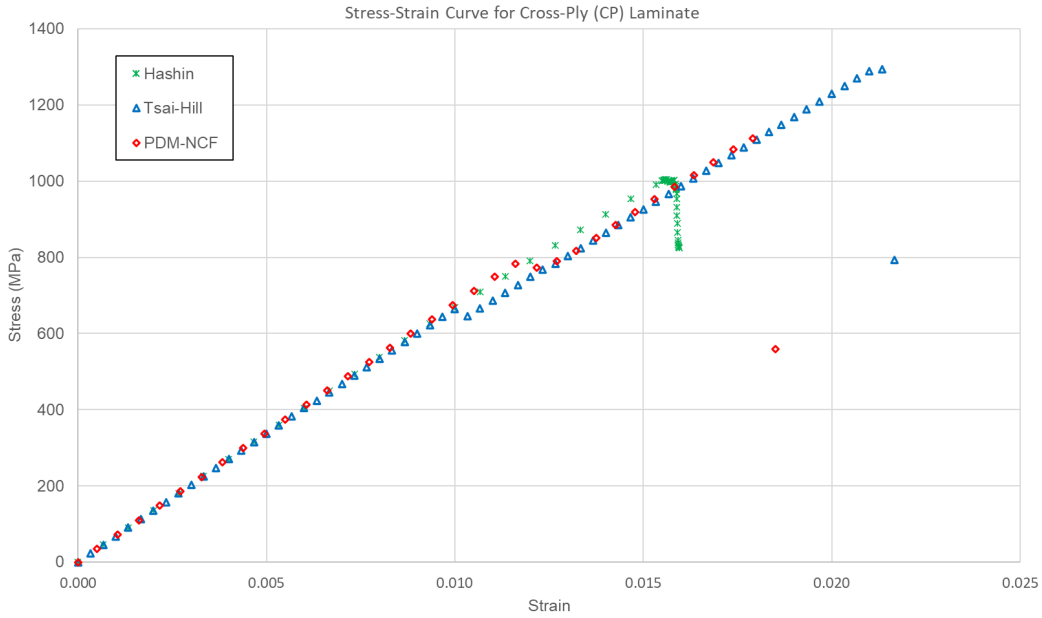

Figure 10: Stress-strain graph with all three damage models for CP laminate

The Tsai-Hill model overestimated the laminate strength by approximately 30%, predicting a failure strain that was 35% higher than the Hashin model. This overestimation is due to the model's inclusion of different stress contributions such as stress in transverse direction, σ_{22} and in-plane shear, τ_{12}, which tends to elevate overall damage initiation level even when these stresses are not dominant in the actual failure mechanism.

For the AP laminates, the reported experimental stiffness and strength are 16 ± 1 GPa and 121 ± 2 MPa, respectively. Due to the AP layup configuration, the laminate's damage is driven predominantly by matrix damage induced by in-plane shear stress, τ_{12}. As shown in Figure 11, both the Hashin and Tsai-Hill models exhibit good agreement with the experimental results, where a strength drop is observed at approximately 120 MPa.
The PDM-NCF predicts a laminate strength of 133 MPa, representing an overestimation of 10% compared to the experimental value. However, this discrepancy is acceptable, as it lies within the experimental tolerance and reflects the inherent characteristics of the model. Specifically, the PDM-NCF incorporates a combination of shear stress components that is contributed by two fracture plane-dependent shear stress terms, namely longitudinal shear stress and transverse shear stress, through a stress transformation as described in Eq. (2).

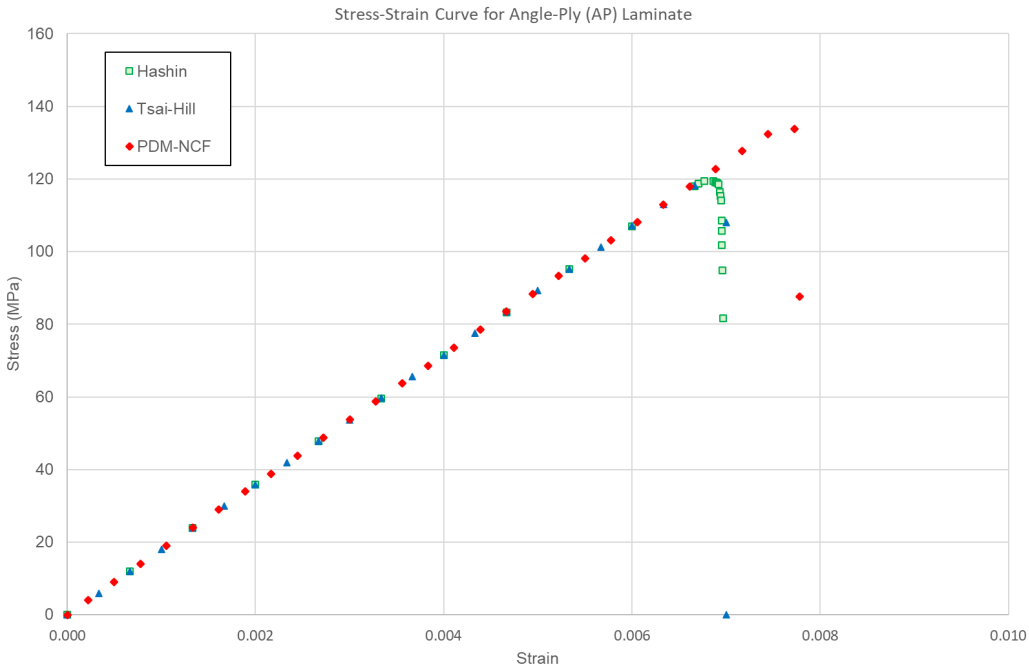

Figure 11: Stress-strain graph with all three damage models for AP laminate.

Additionally, the shear response in all models was assumed to be linear, which represents a simplification of the actual material behavior. In reality, the polymer matrix exhibits non-linear characteristics due to changes in its internal structure. The polymeric chain will undergo a softening process where the chain "straightens" under applied stress, contributing to the observed non-linearity. This behavior could be more accurately captured through by modifying the constitutive equation of the composite laminate. However, such enhancement falls beyond the scope of this study, which focuses on verifying the effectiveness of the proposed model. Table 5 summarizes the prediction results for both laminates across the different damage models. PDM-NCF demonstrates good agreement with experimental values, highlighting its capability in prediction for fiber-driven and matrix-driven damage.

Table 5: Summary of NCF laminate strength prediction

Laminate	Experimental (MPa)	Hashin (MPa)	Tsai-Hill (MPa)	PDM-NCF (MPa)	Error (PDM-NCF vs. Exp)
Cross-Ply (CP)	992 ± 25	1000	1293	1112	12%
Angle-Ply (AP)	121 ± 2	119	118	133	10%

4.2 Damage Initiation Stress and Damage Onset

An essential requirement in developing a reliable damage model is its capability to accurately capture damage initiation stress and its location of onset, particularly for first-ply failure (FPF) analysis. Figure 12 presents the predicted location of damage initiation.

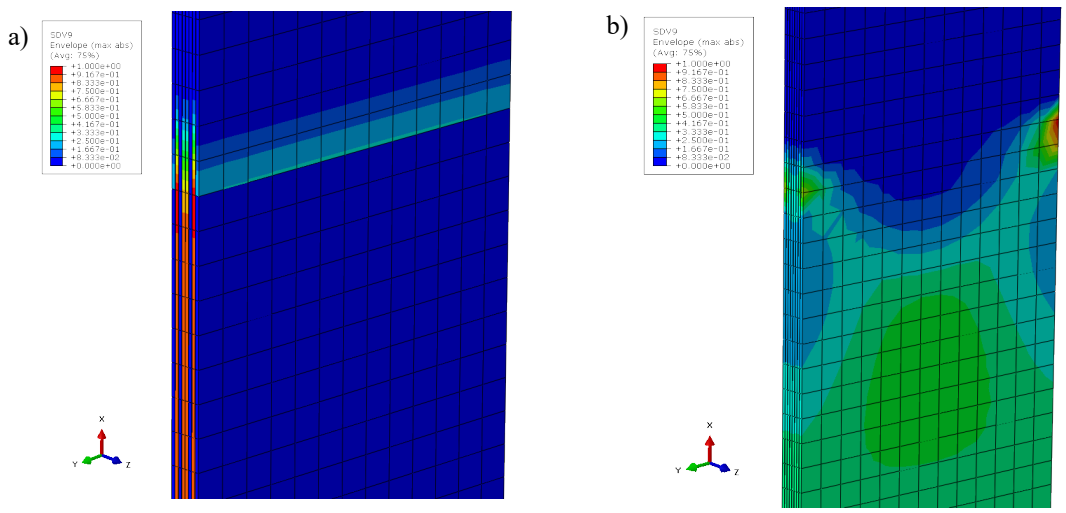

Figure 12: First-ply failure damage onset location for both laminates using PDM-NCF damage model: a) cross-ply laminate and b) angle-ply laminate.

For the CP laminate, the PDM-NCF model predicted a matrix damage initiation stress of 295 MPa. This prediction is slightly higher than the experimental value, likely due to the assumption of in-situ transverse tensile strength employed within the PDM-NCF model. Nonetheless, the numerical results suggest that the model captures the onset of element failure reasonably well. Initial damage was first observed in the 90° plies. The stress concentrated near the gripping point within the gauge length area.

Meanwhile, for the AP laminate, the model predicted a matrix damage initiation stress of 81 MPa, signifying a 16% underestimation compared to the experimental value. This discrepancy may stem from the model's assumption of a linear matrix response, which does not fully capture the inherent non-linear behavior of polymer matrices. The damage initiated at the edge of the specimen, near the gripping area and rapidly propagating along in 45° direction. Table 6 summarizes all other damage model's predictions on the damage initiation stress. The Hashin model demonstrates the closest number to experimental values.

Table 6: Summary of NCF laminate damage initiation stress prediction

Laminate	Experimental (MPa)	Tsai-Hill (MPa)	Hashin (MPa)	PDM-NCF (MPa)	Error (PDM-NCF vs. Exp)
Cross-Ply (CP)	270 ± 3	337	270	295	9%
Angle-Ply (AP)	97 ± 5	118	118	81	-16%

4.3 Propagation of Failure

One of the PDM-NCF key features is its capability to capture and visualize failure propagation. As elements begin to fail, their load-bearing capacity is lost and redistributed to the surrounding elements. This load-redistribution cycle continues progressively, providing a clear representation of how failure propagates through the laminate. This behavior is illustrated in Table 7, which shows the progression of failure for the AP laminate, from damage initiation to complete structural failure.

Table 7: Progression of matrix damage in AP laminate

Strain	Specimen Failure State	Remark
$2.78e^{-3}$		
$3.89e^{-3}$	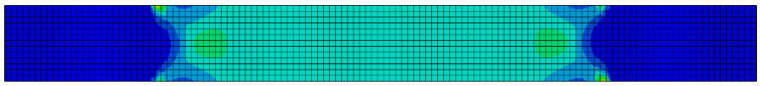	
$5.28e^{-3}$	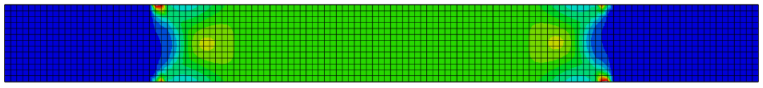	Damage Initiation
$6.67e^{-3}$	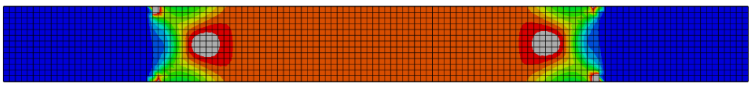	Damage Propagation (internal)
$7.78e^{-3}$	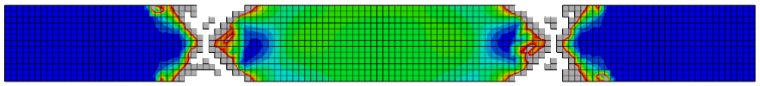	Complete Failure

Failure propagation begins once damage initiates at the edge of gripping area, within the gage length of the specimen. The damage then continues to progress along the 45° direction towards the opposite side of the laminate. This propagation pattern highlights the dominance of shear stress acting on the plies, further confirming a matrix-driven damage mechanism. Eventually, as all load-bearing elements fail and no active element to sustain the load, the laminate undergoes abrupt disintegration, releasing all the fracture energies stored within the system.

5.0 CONCLUSIONS

Unlike conventional UD tape-based composites, the NCF composites are not transversely isotropic due to the presence of resin pocket and fiber waviness as a result from the stitching process, affecting the laminate's mechanical performance. Therefore, an adequate design

tool is essential to properly simulate and predict its behavior. In this paper, a progressive damage model framework for NCF composites is established.

The developed framework integrates strength-based damage criteria and damage evolution model to capture the behavior of NCF composites. From the analysis, the model is capable of simulating the elastic phase, damage initiation and damage evolution with good agreement. The stiffness prediction showed no error for both CP and AP laminates due to same elastic behavior, while the strength prediction showed up to 16% error for AP laminate, believed due to the matrix material non-linearity which was not accounted for in this study.

To conclude, a verified framework for progressive damage modelling of NCF composites has been established and allows for robust prediction of the NCF composites failure. The framework serves as a tool for composite researchers and engineers to deal with NCF fatigue damage under complex three-dimension stress state.

ACKNOWLEDGEMENT

The authors acknowledge the research funding support from Aerospace Malaysia Innovation Centre (AMIC) under the Next-Generation Aerostructure Process (NXAP) research program and University of Technology Malaysia (UTM) for close collaboration in this project.

REFERENCES

[1] G. A. Bibo, P. J. Hogg, R. Backhouse, and A. Mills, "Carbon-fibre non-crimp fabric laminates for cost-effective damage-tolerant structures," *Compos. Sci. Technol.*, vol. 58, no. 1, pp. 129–143, 1998 doi: 10.1016/S0266-3538(97)00106-1.

[2] D. Hartung and M. Wiedemann, "Adaptive, tolerant and efficient composite structures," pp. 167–177, 2013 doi: 10.1007/978-3-642-29190-6.

[3] L. E. Asp, F. Edgren, and S. Anders, "Effects of stitch pattern on the mechanical properties of non-crimp fabric composites," *ECCM11 - 11TH European Conference On Composite Materials, Rhodes, Greece*, 2004.

[4] F. Edgren, D. Mattsson, L. E. Asp, and J. Varna, "Formation of damage and its effects on non-crimp fabric reinforced composites loaded in tension," *Compos. Sci. Technol.*, vol. 64, no. 5, pp. 675–692, 2004 doi: 10.1016/S0266-3538(03)00292-6.

[5] H. Molker, D. Wilhelmsson, R. Gutkin, and L. E. Asp, "Orthotropic criteria for transverse failure of non-crimp fabric-reinforced composites," *J. Compos. Mater.*, vol. 50, no. 18, pp. 2445–2458, 2016 doi: 10.1177/0021998315605877.

[6] F. Edgren, L. E. Asp, and R. Joffe, "Failure of NCF composites subjected to combined compression and shear loading," *Compos. Sci. Technol.*, vol. 66, no. 15, pp. 2865–2877, 2006 doi: 10.1016/j.compscitech.2006.02.021.

[7] F. Edgren, C. Soutis, and L. E. Asp, "Damage tolerance analysis of NCF composite sandwich panels," *Compos. Sci. Technol.*, vol. 68, no. 13, pp. 2635–2645, 2008 doi: 10.1016/j.compscitech.2008.04.041.

[8] E. Marklund, J. Varna, and L. E. Asp, "Stiffness and strength modelling of non-crimp fabric composites," *52nd AIAA/ASME/ASCE/AHS/ASC Struct. Struct. Dyn. Mater. Conf. Denver, USA*, no. April, pp. 1–17, 2011 doi: 10.2514/6.2011-1748.

[9] T. Bru, P. Hellström, and R. Gutkin, "Characterisation of the mechanical and fracture properties of a uni-weave carbon fibre / epoxy non-crimp fabric composite," vol. 6, pp. 680–695, 2016.

[10] H. Molker, R. Gutkin, and L. E. Asp, "Implementation of failure criteria for transverse failure of orthotropic Non-Crimp Fabric composite materials," *Compos. Part A Appl. Sci. Manuf.*, vol. 92, pp. 158–166, 2017 doi: 10.1016/j.compositesa.2016.09.021.

[11] S. T. Pinho, G. M. Vyas, and P. Robinson, "Material and structural response of polymer-matrix fibre-reinforced composites," *J. Compos. Mater.*, vol. 47, no. 6–7, pp. 679–696, 2013 doi: 10.1177/0021998313476523.

[12] A. S. Kaddour, M. J. Hinton, S. Li, and P. A. Smith, "How Can Composites Design and Manufacture Communities Build Their Strength," *ECCM16 - 16TH European Conference On Composite Materials*, Seville, Spain, 22-26 June 2014.
[13] I. Lapczyk and J. A. Hurtado, "Progressive damage modeling in fiber-reinforced materials," *Compos. Part A Appl. Sci. Manuf.*, vol. 38, no. 11, pp. 2333–2341, 2007
doi: 10.1016/j.compositesa.2007.01.017.
[14] L. M. Ferreira and E. Graciani, "Progressive Damage Study of Ncf Composites Under Compressive Loading," *ECCM16 - 16TH European Conference On Composite Materials*, Seville, Spain, 22-26 June 2014.
[15] S. T. Pinho, C. G. Dávila, P. P. Camanho, L. Iannucci, and P. Robinson, "Failure Models and Criteria for FRP Under In-Plane or Three-Dimensional Stress States Including Shear Non-linearity," *Tm-2005-213530*, no. February, p. 68, 2005
doi: NASA/TM-2005-213530.
[16] P. P. Camanho, C. G. Dávila, S. T. Pinho, L. Iannucci, and P. Robinson, "Prediction of in situ strengths and matrix cracking in composites under transverse tension and in-plane shear," *Compos. Part A Appl. Sci. Manuf.*, vol. 37, no. 2, pp. 165–176, Feb. 2006
doi: 10.1016/j.compositesa.2005.04.023.
[17] A. Puck and H. Schu, "Failure Analysis of FRP Lamninates by Means of Physically Based Phenomenological Models.pdf," *Compos. Sci. Technol.*, vol. 62, pp. 1633–1662, 2002
doi: 10.1016/S0266-3538(01)00208-1.
[18] Z. Hashin, "Failure Criteria for Unidirectional Fiber Composites," *J. Appl. Mech.*, vol. 47, no. 2, p. 329, 1980
doi: 10.1115/1.3153664.
[19] Z. P. Bažant and B. H. Oh, "Crack band theory for fracture of concrete," *Matériaux Constr.*, vol. 16, no. 3, pp. 155–177, 1983
doi: 10.1007/BF02486267.
[20] C. Zhang, N. Li, W. Wang, W. K. Binienda, and H. Fang, "Progressive damage simulation of triaxially braided composite using a 3D meso-scale finite element model," *Compos. Struct.*, vol. 125, pp. 104–116, Jul. 2015
doi: 10.1016/j.compstruct.2015.01.034.
[21] G. Duvaut and J. L. Lions, *Inequalities in Mechanics and Physics*, vol. 219. Berlin, Heidelberg: Springer Berlin Heidelberg, 1976.
[22] P. Maimí, P. P. Camanho, J. A. Mayugo, and C. G. Dávila, "A continuum damage model for composite laminates: Part II - Computational implementation and validation," *Mech. Mater.*, vol. 39, no. 10, pp. 909–919, 2007
doi: 10.1016/j.mechmat.2007.03.006.
[23] R. Vignjevic, N. Djordjevic, T. De Vuyst, and S. Gemkow, "Modelling of strain softening materials based on equivalent damage force," *Comput. Methods Appl. Mech. Eng.*, vol. 335, pp. 52–68, 2018
doi: 10.1016/j.cma.2018.01.049.
[24] K. Vallons, I. Duque, S. V. Lomov, and I. Verpoest, "Loading direction dependence of the tensile stiffness, strength and fatigue life of biaxial carbon/epoxy NCF composites," *Compos. Part A Appl. Sci. Manuf.*, vol. 42, no. 1, pp. 16–21, 2011
doi: 10.1016/j.compositesa.2010.09.009.
[25] S. S. R. Koloor, M. R. Ayatollahi, and M. N. Tamin, "Elastic-damage deformation response of fiber-reinforced polymer composite laminates with lamina interfaces," *J. Reinf. Plast. Compos.*, vol. 36, no. 11, pp. 832–849, 2017
doi: 10.1177/0731684417693427.
[26] S. S. R. Koloor, M. R. Khosravani, R. I. R. Hamzah, and M. N. Tamin, "FE model-based construction and progressive damage processes of FRP composite laminates with different manufacturing processes," *Int. J. Mech. Sci.*, vol. 141, no. February, pp. 223–235, 2018
doi: 10.1016/j.ijmecsci.2018.03.028.